pharmaceutics

MDPI

Article

Enhancing the Solubility of Co-Formulated Hydrophobic Drugs by Incorporating Functionalized Nano-Structured Poly Lactic-*co*-glycolic Acid (*nf*PLGA) During Co-Precipitation

Mohammad Saiful Islam and Somenath Mitra *

Department of Chemistry and Environmental Science, New Jersey Institute of Technology, Newark, NJ 07102, USA; mi238@njit.edu

* Correspondence: somenath.mitra@njit.edu

Abstract: Background/Objectives: The co-formulation of active pharmaceutical ingredients (APIs) is a growing strategy in biopharmaceutical development, particularly when it comes to improving solubility and bioavailability. This study explores a co-precipitation method to prepare co-formulated crystals of griseofulvin (GF) and dexamethasone (DXM), utilizing nanostructured, functionalized polylactic glycolic acid (*nf*PLGA) as a solubility enhancer. **Methods**: An antisolvent precipitation technique was employed to incorporate *nf*PLGA at a 3% concentration into the co-formulated GF and DXM, referred to as DXM-GF-*nf*PLGA. The dissolution performance of this formulation was compared to that of the pure drugs and the co-precipitated DXM-GF without *nf*PLGA. **Results**: Several characterization techniques, including electron microscopy (SEM), RAMAN, FTIR, TGA, and XRD, were used to analyze the *nf*PLGA incorporation and the co-precipitated co-formulations. The inclusion of *nf*PLGA significantly enhanced the dissolution and initial dissolution rate of both GF and DXM in the DXM-GF-*nf*PLGA formulation, achieving a maximum dissolution of 100%, which was not attained by the pure drugs or the DXM-GF formulation. The incorporation of *nf*PLGA also reduced the amount of time taken to reach 50% (T_{50}) and 80% (T_{80}) dissolution. T_{50} values decreased from 52 and 82 min (for pure DXM and GF) to 23 min for DXM-GF-*nf*PLGA, and the T_{80} improved to 50 min for DXM-GF-*nf*PLGA, significantly outpacing the pure compounds. Furthermore, incorporating *nf*PLGA into the crystal structures greatly accelerated the dissolution rates, with initial rates reaching 650.92 µg/min for DXM-GF-*nf*PLGA compared to 540.60 µg/min for DXM-GF, while pure GF and DXM showed lower rates. **Conclusions**: This work demonstrates that *nf*PLGA incorporation enhances dissolution performance by forming water channels within the API crystal via hydrogen-bonding interactions. This innovative *nf*PLGA incorporation method holds promise for developing hydrophobic co-formulations with faster solubility and dissolution rates.

Keywords: co-formulation; functional *nf*PLGA; incorporation; antisolvent technology; co-precipitation; dissolution; aqueous solubility

Academic Editors: Anderson R. L. Caires, William Facchinatto, Regiane Godoy de Lima and Juan Torrado

Received: 14 November 2024
Revised: 3 January 2025
Accepted: 7 January 2025
Published: 8 January 2025

Citation: Islam, M.S.; Mitra, S. Enhancing the Solubility of Co-Formulated Hydrophobic Drugs by Incorporating Functionalized Nano-Structured Poly Lactic-*co*-glycolic Acid (*nf*PLGA) During Co-Precipitation. *Pharmaceutics* **2025**, *17*, 77. https://doi.org/10.3390/pharmaceutics17010077

1. Introduction

Solubility plays a critical parameter in drug delivery [1,2], especially for drugs classified under Biopharmaceutical Classification System (BCS) Class II and IV [3,4] due to their poor solubility and low bioavailability [5,6]. These compounds constitute a substantial proportion—approximately 40 to 70 percent [7]—of new drug entities (NCE)/candidates in development stages [8–10]. Consequently, significant hurdles may be encountered while

designing and delivering such drug products, particularly when it comes to formulating strategies to overcome solubility or permeability challenges [10,11]. Low solubility often results in unstable therapeutic concentrations, necessitating the implementation of developmental strategies [12] to enhance drug solubility and permeability [1,13,14]. Consequently, optimizing drug solubility can significantly contribute to improved therapeutic outcomes [15].

Significant efforts have been dedicated to overcoming the solubility challenges of hydrophobic drugs [16]. Conventional techniques for solubility enhancement include particle size reduction [17] through methods like micronization [18] and nanoparticle formation [10,19,20], solid dispersion techniques [21], co-solvents [22], complexation [23], salt formation [24], pH adjustment [25], surfactant use [26], hydrotropic [27], lipid-based formulations [28], nano-emulsions [29], spray drying [30], and solvent selection [17,31]. Formulations with solubilizing agents such as polymers and surfactants have also been used for dissolution enhancement [32]. Additionally, various materials like nanostructured dendrimers, micelles, carbon nanotubes, graphene, graphene oxide, quantum dots [33,34], proteins [35], viruses [36], ceramics [37,38], metals, semiconductors [39], lipids [28], polymeric thin films [40], hydrogels [41], and amorphous or crystalline surfaces are utilized in different types of drug formulations to enhance their solubility [42,43].

Co-formulation presents an attractive strategy that combines multiple drugs into a single oral solid or injectable product [44,45]. For poorly soluble drug components, co-formulation has been shown to enhance bioavailability [44,46]. Additionally, it is useful for developing combination therapies [47,48]. Recent advancements in this field include approved fixed-dose combinations like Pertuzumab, Trastuzumab, and Hyaluronidase for HER-2-positive breast cancer [49], stable formulations combining durvalumab (Imfinzi®, anti-PD-L1) and tremelimumab (anti-CTLA-4) [50], as well as co-formulated stable solid dispersions of Artemether (ARTM) and Lumefantrine (LUMF) using optimized drug–polymer–surfactant blends via hot-melt extrusion [51], and spherical cocrystallization via direct compression to improve solubility and bioavailability [52]. Co-formulated drugs can streamline treatment protocols, optimize drug delivery, and reduce manufacturing costs [44]. Moreover, co-formulated drug formulations hold clinical potential for treating complex diseases. Previous research has shown that multiple drugs can work synergistically within the GI-to-blood circulation system, minimizing adverse effects [53]. This supports the idea that co-formulation strategies are crucial for modern pharmaceutical development [54].

Co-formulation via co-precipitation can promote intermolecular interactions at the molecule's surfaces, leading to faster solubility and improved bioavailability profiles [55]. Thus, co-precipitation can enhance the physicochemical properties of combined hydrophobic drugs [56,57]. Co-formulation that involves the antisolvent precipitation technique is promising for drug-delivery research [58]. Our previous study has explored incorporating graphene oxide (nGO) [59], carbon nanotubes [60], functionalized nanostructured polylactic acid (PLA) [61], and polylactic glycolic acid (PLGA) [62] into hydrophobic APIs to enhance dissolution. Although nGOs have hydrophilic functional groups on their surfaces, facilitating interaction with water to enhance dissolution [63,64], they are not FDA-approved and may pose toxicity risks. Alternatively, we have investigated the use of functionalized nanoparticles of PLGA [65], referred to as *nf*PLGA. They are not water-soluble by themselves, but contain hydrophilic functionalized groups on their surfaces [66,67], such as carboxyl and/or hydroxyl, which promote the aqueous solubility of the insoluble drug crystals through hydrophilic interactions. This incorporation helps to facilitate faster dissolution.

The objective of this research is to incorporate *nf*PLGA to co-precipitate the hydrophobic API co-formulations to fabricate drug–drug-*nf*PLGA composites with enhanced dissolution properties. Antifungal Griseofulvin, which is a BCS II highly hydrophobic drug with a solubility of 0.00864 mg/L [68], and dexamethasone (DXM), which is a BCS-IV classified corticosteroidal and anti-inflammatory, 9-fluoro-glucocorticoid drug that is practically insoluble in water with a solubility profile of 0.080 mg/mL [69,70], are used to form co-formulated composites with enhanced solubility. The combination of an antifungal drug and a steroid is commonly used to treat infections accompanied by inflammation, making this combination highly significant from a therapeutic standpoint.

2. Materials and Methods

2.1. Materials

Griseofulvin and dexamethasone were purchased from Sigma Aldrich (St. Louis, MO, USA). Poly lactic-*co*-glycolic acid polymer was purchased from Polysciences Inc. (Warrington, PA, USA). Acetone was bought from Sigma Aldrich, and sulfuric acid and nitric acid were bought from Fisher Scientific supplier (Thermo Fisher Scientific Inc., Waltham, MA, USA). The source of 1-Octanol was also Sigma Aldrich (St. Louis, MO, USA), and the purified Milli-Q water was collected from NJIT York centers Milli-Q plus system.

2.2. Fabrication of nfPLGA

Synthesis of *nf*PLGA particles was carried out following a previously published method [61,62]. A multimode microwave-accelerated reaction system, specifically the CEM Microwave Reactor (MARS-5, Matthews, NC, USA), was used for the acid oxidation of PLGA. Ground PLGA polymer was mixed with a 1 M concentration of sulfuric acid (H_2SO_4) and nitric acid (HNO_3) solution in a 3:1 ratio. This mixture comprised 200 mg of PLGA and 60 mL of the acid solution.

The acid-dispersed PLGA mixture was transferred to a microwave sample holder, which was then tightly closed and sealed to ensure an airtight environment. The microwave reactor was operated under specific conditions: a standard control type program, power set to 800 W at 80% intensity, temperature maintained at 60 °C, and pressure at 200 psi. The reaction was allowed to run for 60 min, with a hold time of 10 min.

After completing the 60 min microwave-accelerated reaction, the acid-treated and microwave-irradiated PLGA samples were vacuum-filtered through a 0.2-micron PTFE membrane filter, washed with milli-Q water, and vacuum-dried for 48 h. Once dried, the functionalized PLGA powder/crystalline particles were dispersed in milli-Q water. This dispersion was then subjected to sonication using a probe sonicator. The samples were sonicated in 60 min intervals while maintaining a controlled temperature to ensure that the sample temperature remained at room temperature. The resulting sonicated particles are referred to as *nf*PLGA.

2.3. Preparation of Co-Formulated DXM-GF-nfPLGA

An antisolvent precipitation method was employed to precipitate co-formulated drugs, specifically DXM-GF and DXM-GF-*nf*PLGA composites, following a previously outlined process [59,60]. Acetone was used to dissolve the 200 mg of DXM and 200 mg of GF containing DXM-GF mixture (1:1), while *nf*PLGA (12 mg), a nano-functionalized polymer, was dissolved in acetone to produce a clear polymer solution. The DXM-GF mixture in acetone was subjected to bath sonication, and the polymer solution was gradually added dropwise into the drug mixture. This process of adding the polymer and continuing sonication for up to 10 min ensured proper mixing of the components. Afterward, the combined drug solution was removed from the sonication bath and left at room temperature

for 30 min to stabilize. Subsequently, the co-formulation was placed in an ice bath, and milli-Q water was added dropwise to induce the antisolvent effect. The milli-Q water acted as the antisolvent, and after sufficient addition, a milky suspension of the DXM-GF-*nf*PLGA co-formulation was formed, which later resulted in the precipitation of a bulk amount of the product. The precipitated particles were then filtered using a 0.2-micron PTFE membrane filter and vacuum-dried in an oven at room temperature for 48 h to achieve finely dried particles. Additionally, the co-formulation without *nf*PLGA (DXM-GF) was prepared separately to distinguish the effects of *nf*PLGA incorporation.

2.4. Characterization of Co-Formulated DXM-GF-nfPLGA

Various analytical characterization techniques were employed to investigate and characterize the formulated work. The hydrodynamic Z-average size and zeta potential of the functionalized and nano-sized *nf*PLGA particles were measured using a Dynamic Light Scattering (DLS) system (Malvern Nano ZS, Model: ZEN 3600, Worcestershire, UK). A JEOL JSM-7900F scanning electron microscope (SEM) (JEOL, Tokyo, Japan) was utilized to image the drug crystal formulations, and the samples were carbon-coated using an EMS Quorum coater. Optimized operating conditions were applied during SEM imaging, including a 10 mm working distance and an accelerating voltage of 5 kV. Aztec software (AZtecLive 5.1) was used to produce the elemental identification and elemental mapping of the co-formulation.

A PerkinElmer 8000 Model TGA instrument (Shelton, CT, USA) was used to analyze the decomposition profile of the co-formulated drugs and quantify *nf*PLGA incorporation. For the TGA, approximately 10 mg of powder samples were placed in a ceramic sample holder and heated in a furnace under a nitrogen flow rate of 20 mL/min. The heating rate was set to 10 °C/min, and the temperature ranged from 30 to 700 °C. The melting point and purity of the co-formulated drugs were determined using a Differential Scanning Calorimeter (PerkinElmer DSC 6000, Shelton, CT, USA). In the DSC analysis, the operating temperature was between 30 and 300 °C at a 10 °C/min heating rate, and the sample amount was between 5 and 10 mg. Raman spectral intensity was measured with a ThermoFisher Scientific DXR2xi Raman imaging microscope instrument (Madison, WI, USA), employing a 532 nm laser wavelength and full-frequency acquisition mode 3800–200 cm^{-1} region. Powder X-ray diffraction (PXRD) was performed to confirm the crystalline identity of the co-formulated drugs using the PANalytical EMPYREAN XRD (Malvern, UK) instrument with a Cu Kα radiation source. The diffraction intensity was recorded over a 2θ range of 5–70°. A HighScore Plus (version 5.2) software was used for analysis. Fourier-transform infrared (FTIR) analysis was performed (using diamond ATR) with an Agilent Cary 670 Benchtop spectrometer (Santa Clara, CA, USA) to assess the functional properties of the drugs and their co-formulation. The analysis was conducted with ResolutionsPro (version 5.4.0.3389) software, utilizing 64 scans per sample and a resolution of 4 cm^{-1}.

The aqueous solubility of the drug samples was determined as follows. The drug formulation (50 mg) in 100 mL milli-Q water in a glass vial was stirred in water for 24 h using a magnetic stirrer to reach equilibrium [71,72]. Afterward, the mixture was filtered, and the resulting solution was analyzed via UV absorption. The octanol–water partition coefficient was measured as follows. For this experiment, 50 mg of the drug sample was added to a 1:1 mixture (50 mL each) of water (aqueous phase) and octanol (organic phase) for octanol–water partitioning. The mixture was stirred for one hour to allow for partitioning between the organic and aqueous phases and to achieve equilibrium. Afterward, ultracentrifugation separated the two phases, and the aqueous phase was collected. The drug concentration in the aqueous phase was then determined using a UV-Vis

spectrometer, and the concentration in the octanol phase was determined by subtracting the aqueous phase value. Then, the logP was calculated based on these concentrations [73,74].

The in vitro dissolution test for the co-formulated drugs was conducted using the USP apparatus II paddle system with sink condition, in accordance with the United States Pharmacopeia (USP) dissolution method ⟨711⟩ [75–77]. The dissolution performance was assessed using the Symphony 7100 Distek instrument (North Brunswick, NJ, USA) following the established protocol. Simulated gastric fluid (SGF), prepared to mimic stomach conditions at pH 1.4, was used as the dissolution medium. This was achieved by mixing 900 mL of 0.1 N HCl to obtain the desired pH, which was then added to the dissolution bath. The experiment was performed under optimized conditions, including a temperature of 37 ± 0.5 °C and a paddle rotation speed of 75 rpm, over a 4 h duration. Samples were collected at predetermined intervals. Drug particles (100 mg) were initially dispersed in a small volume of water and introduced into the dissolution bath using a syringe, allowing them to circulate freely in the medium. Aliquots of approximately 2 mL were withdrawn at time points of 5, 10, 20, 30, 50, 80, 120, 150, 180, and 240 min. The collected samples were filtered through 0.2-micron sterile PTFE syringe filters and transferred into cuvettes for UV-Vis analysis. Drug concentrations were quantified using an Agilent 8453 UV-Vis spectrophotometer (Santa Clara, CA, USA), with calibration performed at 240 nm and 295 nm.

3. Results and Discussion

3.1. Characteristics of DXM-GF-nfPLGA

The SEM images of pure GF, DXM, DXM-GF, and DXM-GF-*nf*PLGA composites are presented in Figure 1a–d. It is evident from Figure 1c that the crystal structure of the single drug GF and DXM remains intact within the physical integration, and the *nf*PLGA attaches to the surface of the co-formulated drugs. Additionally, the *nf*PLGA particles are expected to provide hydrophilic linkages over the drug surfaces, which may produce a water channel to the co-formulated drugs that will lead to high dispersibility and aqueous solubility. The analyses suggest that the co-formulated drugs can retain their structural and morphological integrity upon *nf*PLGA incorporation during the antisolvent process.

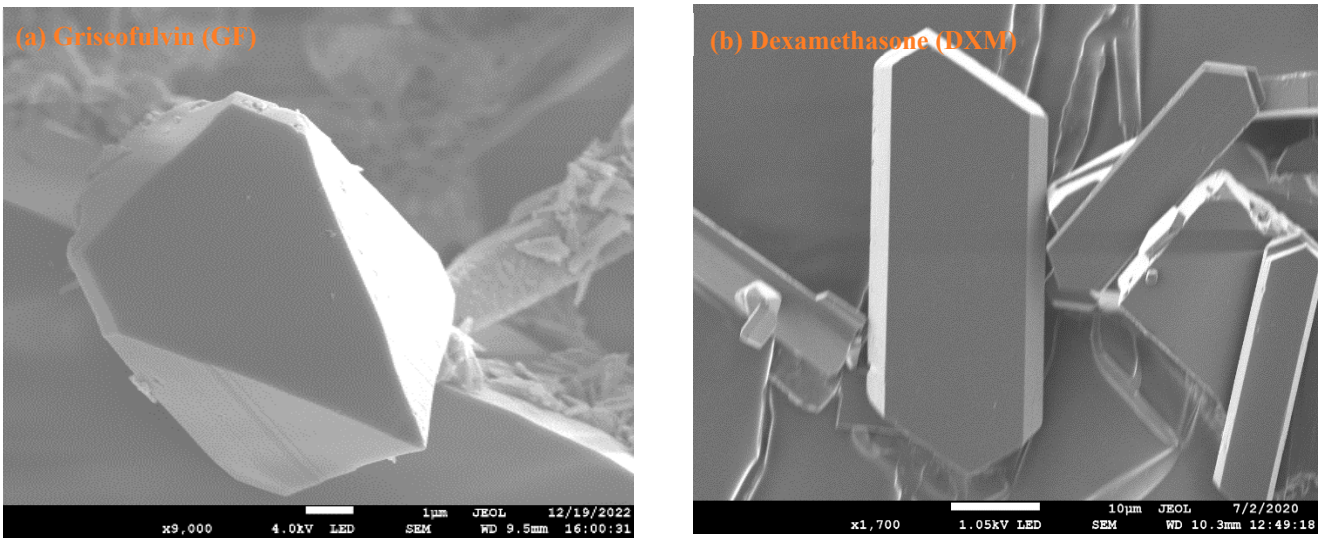

Figure 1. *Cont.*

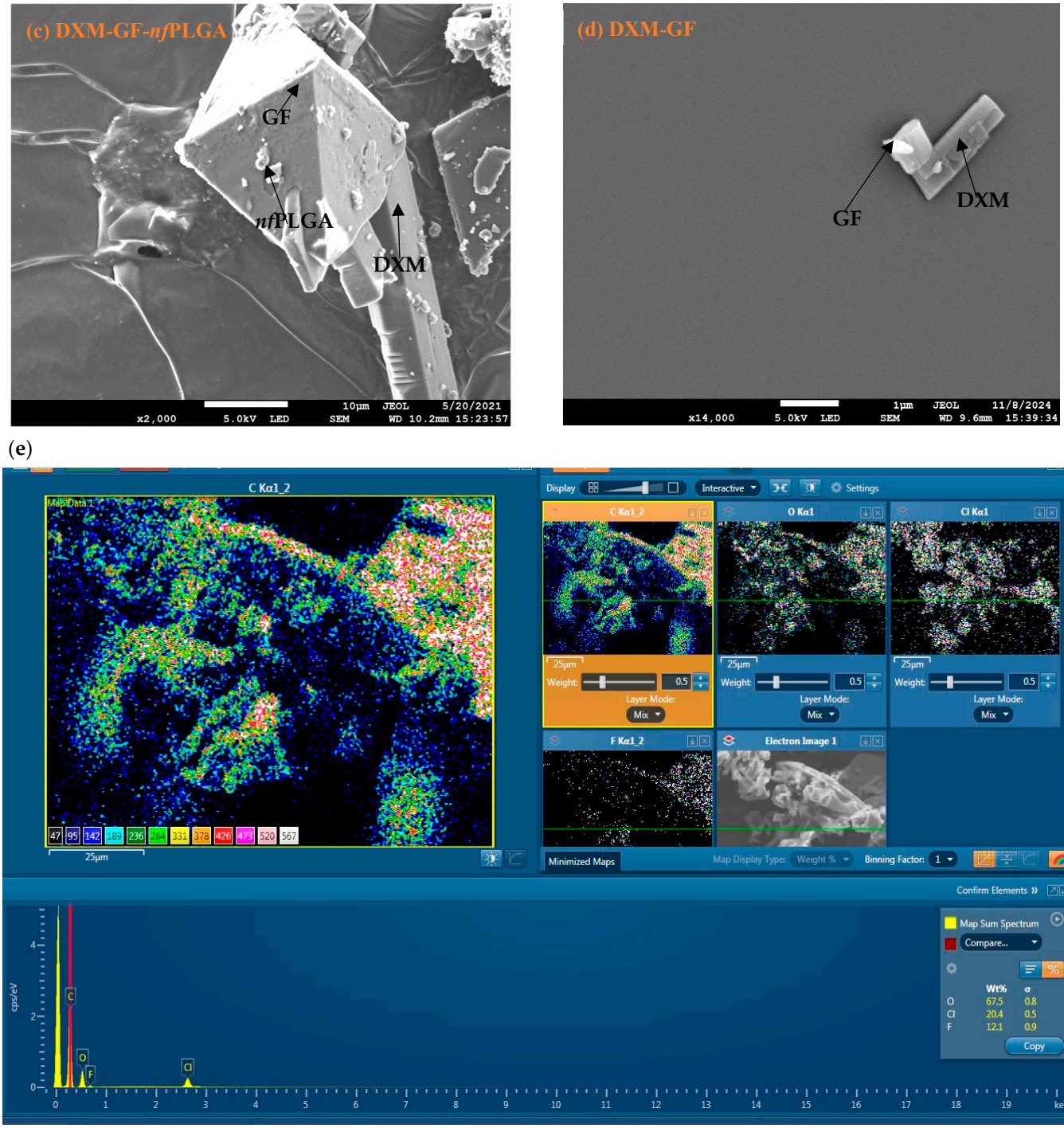

Figure 1. SEM images of (**a**) Pure GF, (**b**) pure DXM, (**c**) DXM-GF-*nf*PLGA co-formulation (carbon coated), (**d**) DXM-GF, and (**e**) EDS elemental mapping for co-formulation of DXM-GF-*nf*PLGA.

The elemental point ID and mapping (EDS) analysis, illustrated in Figure 1e, confirms the distribution of constituent elemental concentrations within the co-formulations derived from individual drugs [78,79]. The analysis reveals the presence of oxygen at 67.5 wt% (from both GF and DXM), chlorine at 20.4 wt% (from GF), and fluorine at 12.1 wt% (from DXM). The figure displays a color legend with distinct color codes corresponding to numerical values, indicating the concentration gradient of specific elements or a combination of elements from lowest to highest. Furthermore, the EDS mapping highlights two distinct crystals that appear to be stacked or attached.

Table 1 presents the water solubility and octanol–water partition coefficient (log P) of the drugs and their co-formulated counterparts. The solubility of the co-formulated drugs with incorporated *nf*PLGA was 0.064 mg/mL, surpassing that of DXM-GF. Furthermore, the log P for the co-formulated drugs was 1.15, indicating a moderately low value due to the enhanced hydrophilicity provided by *nf*PLGA incorporation. The data in Table 1 also reveal that DXM-GF-*nf*PLGA demonstrated an increased zeta potential of −30.2 mV, reflecting improved stability in the aqueous medium. This enhanced stability is attributed to the surface charge of *nf*PLGA particles in the dispersion. Conversely, the pure drugs or DXM-GF alone exhibited a lower zeta potential of −19.7 mV, underscoring their limited ability to achieve similar stability.

Table 1. Physicochemical properties of the formulated drugs' co-formulation.

Formulations	Aqueous Solubility (μg/mL)	Zeta Potential (mV)	logP	Melting Point (°C)
Pure DXM	89.00	−17.2	1.96	261.74
Pure GF	8.64	−15.4	2.16	222.10
DXM-GF	83.70	−19.7	1.75	258.12 (DXM) 203.71 (GF)
DXM-GF-*nf*PLGA	128.70	−30.2	1.15	242.41 (DXM) 212.54 (GF)

An important consideration was whether the DXM or GF structure was altered during the co-formulation process. Figures 2–4 display the XRD, Raman, and FTIR spectral intensity analysis of pure DXM, GF, DXM-GF, and DXM-GF-*nf*PLGA co-formulations. Raman spectra showed distinct peaks for dexamethasone at the C-F stretch (769 cm^{-1}) and for griseofulvin at the C–Cl stretch (651 cm^{-1}), both of which were present in the co-formulation, indicating that their polymorphism remained unchanged. Additionally, X-ray diffraction (XRD) of the co-formulated drugs revealed intensity peaks at different 2θ angles (Supplementary Files contain detailed XRD analysis) corresponding to those of DXM and GF, further supporting the idea that their crystallinity was not altered. In the Fourier-transform infrared spectroscopy (FTIR) analysis, characteristic absorption bands for GF, such as C–O–C (1213 cm^{-1}) and C–Cl (800 cm^{-1}), as well as for DXM, including –O–H (3448 cm^{-1}), C=O (1662 cm^{-1}), and C–F (1056 cm^{-1}), were detected in the co-formulated drugs. Importantly, no changes were observed in the characteristic functional group intensities of the individual drugs after co-formulation. FTIR analysis thus confirmed the presence of both DXM and GF in the co-formulated products, with no significant structural alterations.

In Figure 5a, thermogravimetric analysis (TGA) was used to study the *nf*PLGA incorporation into the co-formulated drugs. The analysis shows that the major decomposition temperature for the co-formulation occurred between 250 and 400 °C. The final formulation contained 66% GF, 31% DXM, and 3% *nf*PLGA. The DXM-GF without *nf*PLGA incorporation contained 60% GF and 40% DXM. Figure 6 shows the differential scanning calorimetry (DSC) for the co-formulated drugs' endothermic peak and the melting point measurement. The DSC thermograms showed a change in the heat capacity and the glass transition at approximately 82 °C and 84 °C [80], followed by a slightly lower endothermic crystallization peak shift between 242.24 °C (DXM) and ~212.5 °C (GF), respectively, from the original drug [81]. The presence of *nf*PLGA and co-precipitation of the two drugs appear to alter the melting points (Table 1) slightly.

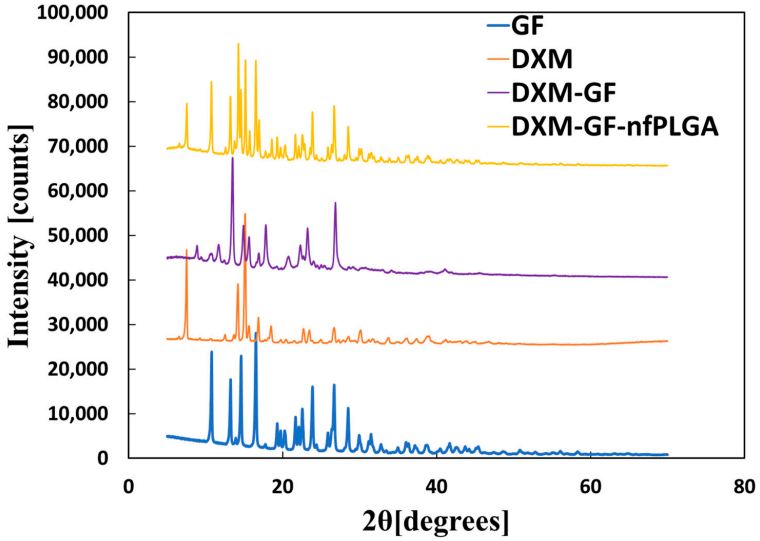

Figure 2. X-ray diffraction (XRD) analysis data for co-formulated drugs' formulation.

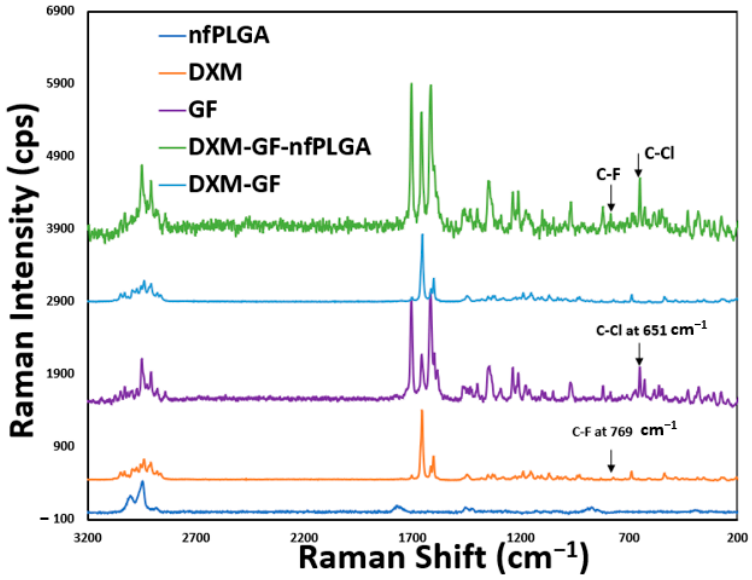

Figure 3. RAMAN analysis data for co-formulated drugs' formulation.

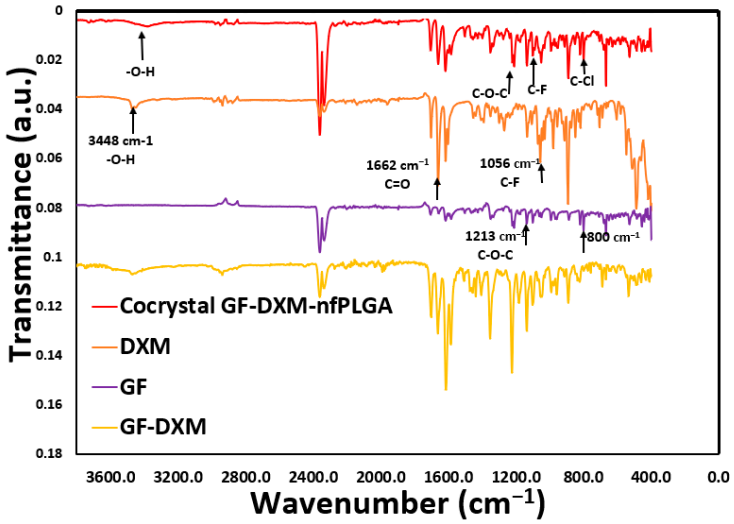

Figure 4. FTIR analysis of co-formulation of drug formulations.

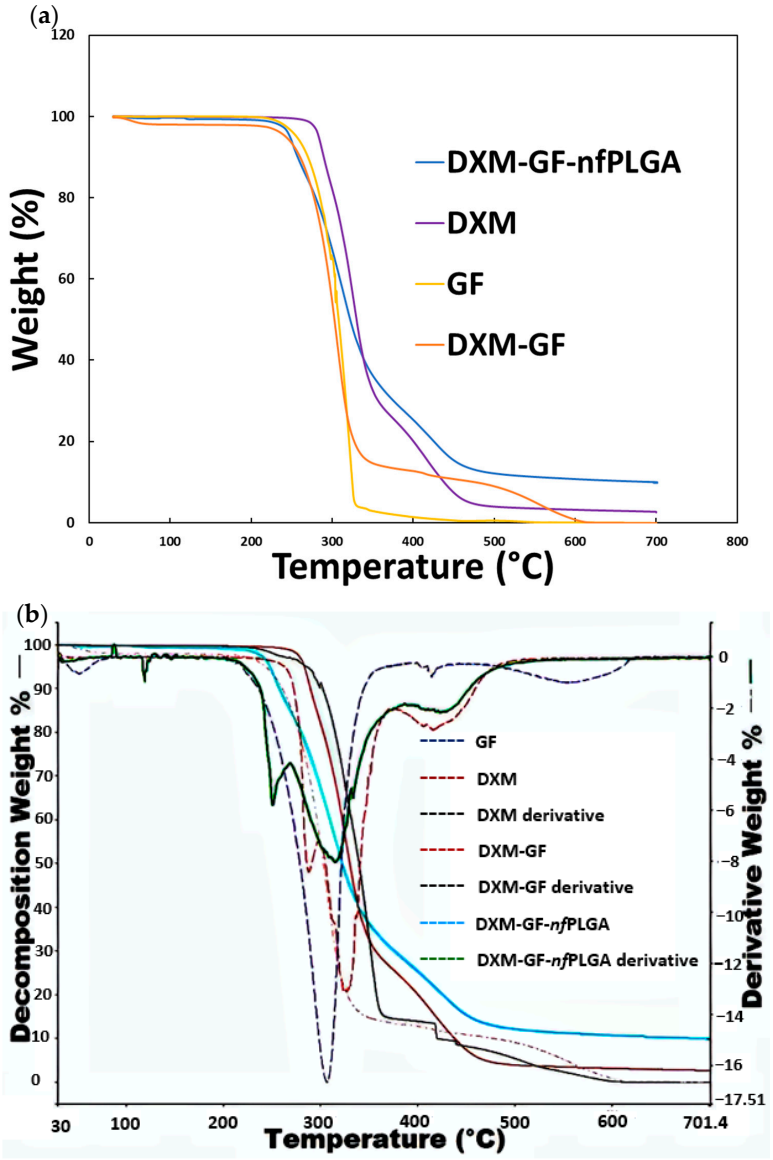

Figure 5. (**a**) TGA of the co-formulated drugs to determine the percentage of *nf*PLGA incorporation and (**b**) antisolvent crystal GF and DXM % from first-derivative curve analysis.

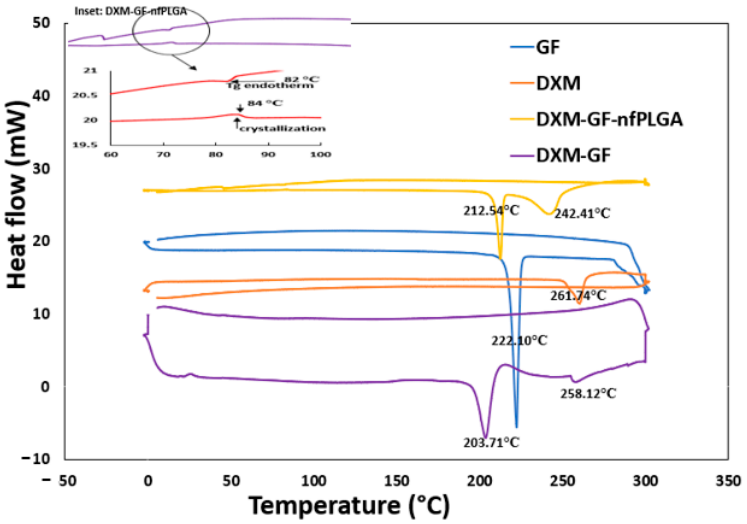

Figure 6. DSC analysis of pure compounds and co-formulations.

3.2. In Vitro Drug Dissolution Analysis

The in vitro drug dissolution and release tests were performed in accordance with the USP-42 dissolution protocol. In this procedure, 0.1 N HCl with a pH of 1.4 was used as the dissolution medium to simulate gastric conditions. The improved dissolution observed in the *nf*PLGA-incorporated drugs and/or co-formulated drug formulations is hypothesized to result from the hydrophilic surface properties of *nf*PLGA, which facilitate interactions with drug molecules, leading to the formation of inter- and intramolecular hydrogen bonds.

Figure 7a is the dissolution profile for DXM, GF, DXM-GF, and DXM-GF-*nf*PLGA. It is evident that *nf*PLGA incorporation led to an enhanced dissolution rate and aqueous solubility, which was attributed to intermolecular interaction with water. The maximum dissolution for GF and DXM reached 100% in DXM-GF-*nf*PLGA, which was not achievable for the pure DXM, GF, or DXM-GF. DXM-GF showed some enhancement over the pure drugs but was still significantly lower than DXM-GF-*nf*PLGA.

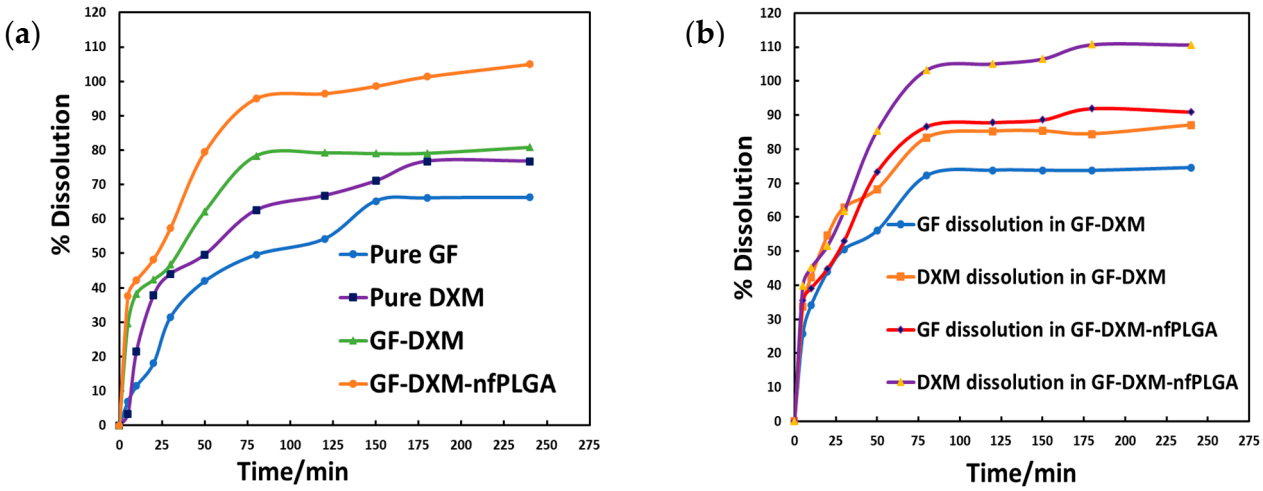

Figure 7. (**a**) Dissolution profile of co-formulated drugs and (**b**) % of individual drug dissolution profile into the co-formulated drugs.

Table 2 presents key dissolution property data, including the improved initial dissolution rate and the time required to achieve 50% dissolution (T_{50}) and 80% dissolution (T_{80}), respectively. Pure DXM and GF had poor water solubility; the T_{50} was 52 and 82 min, respectively. DXM-GF and DXM-GF-*nf*PLGA showed enhanced dissolution compared to the pure APIs; the overall T_{50} in DXM-GF was 34 min, whereas GF and DXM had T_{50}s of 29 and 19 min, respectively. With DXM-GF-*nf*PLGA, the overall T_{50} reduced to 23 min, while those of GF and DXM were 27 and 18 min, respectively. The enhancement was most marked for T_{80}, where pure DXM and GF never reached 80% dissolution, and in DXM-GF, only DXM could achieve an 80% dissolution mark. However, DXM-GF-*nf*PLGA showed an excellent overall T_{80} of 50 min, where GF was at 61 min and DXM at 44 min. The initial rate of dissolution was also an important consideration. Pure GF and DXM had initial dissolution rates of 110.27 µg/min and 180.90 µg/min, respectively. The co-formulated DXM-GF showed an initial dissolution rate of 540.60 µg/min, with GF and DXM at 220.61 µg/min and 290.74 µg/min, respectively. However, the initial dissolution rate was significantly enhanced by the incorporation of *nf*PLGA and reached as high as 650.92 µg/min, with 266.81 µg/min for GF and 325.74 µg/min for DXM.

Table 2. The dissolution profile of the co-formulated drugs.

Formulations	50% Dissolution Time (T_{50})	80% Dissolution Time (T_{80})	Initial Dissolution Rate [0 to 20 min] (μg/min)	Maximum Dissolution (%)
Pure GF	82	Undissolved	110.27	66.2
Pure DXM	52	Undissolved	180.90	76.8
DXM-GF	34	100	540.60	81.0
GF in DXM-GF	29	Undissolved	220.61	74.55
DXM in GF-DXM	19	72	290.74	87.05
DXM-GF-*nf*PLGA	23	50	650.92	105
GF in DXM-GF-*nf*PLGA	27	61	266.81	90.9
DXM in DXM-GF-*nf*PLGA	18	44	325.74	110.6

4. Conclusions

This research presents a novel approach to pharmaceutical formulation, leveraging nano-functionalized PLGA (*nf*PLGA) to enhance the dissolution and potentially improve the bioavailability of hydrophobic co-formulated drugs. By combining antisolvent precipitation technology with *nf*PLGA hydrophilic functionalization achieved through microwave-induced oxidation, this study offers an innovative solution to the persistent challenge of poor drug solubility. The findings demonstrate that the DXM-GF-*nf*PLGA co-formulation achieved complete dissolution (100%) for both GF and DXM, exhibiting superior dissolution kinetics compared to formulations without *nf*PLGA. The incorporation of *nf*PLGA not only reduced the time spent in the gastric environment but also significantly shortened the amount of time taken to reach 50% and 80% dissolution (T_{50} and T_{80}) while improving the initial dissolution rate, addressing a critical obstacle in drug delivery for poorly soluble drugs.

A comprehensive suite of characterization techniques, including XRD, Raman spectroscopy, FTIR, SEM, and in vitro dissolution tests, was employed to assess the structural, morphological, and dissolution properties of the DXM-GF-*nf*PLGA formulation. The results reveal that the inclusion of *nf*PLGA and the multi-drug antisolvent precipitation method markedly enhance solubility and dissolution, likely improving bioavailability. Accelerated initial dissolution rates further confirm that *nf*PLGA plays a pivotal role in enhancing aqueous solubility through hydrogen-bonding interactions, facilitating the formation of water channels. This work validates the hypothesis that *nf*PLGA is an effective agent for promoting faster solubility and dissolution of hydrophobic drugs in co-formulations, offering significant potential for pharmaceutical applications and addressing a major limitation in drug development.

Supplementary Materials: The following supporting information can be downloaded at: https://www.mdpi.com/article/10.3390/pharmaceutics17010077/s1, Coformulation XRD analysis.

Author Contributions: Conceptualization, M.S.I. and S.M.; methodology, M.S.I. and S.M.; validation, S.M. and M.S.I.; formal analysis and investigation, M.S.I. and S.M.; resources, S.M; writing—original draft preparation, M.S.I.; writing—review and editing, M.S.I. and S.M.; supervision, S.M.; funding acquisition, S.M. All authors have read and agreed to the published version of the manuscript.

Funding: This work was partially supported by a U.S. National Science Foundation Accelerating Research Translation cooperative agreement (TIP-2331429) and the NJIT Center for Translational Research. The opinions, findings, and conclusions or recommendations expressed are those of the author(s) and do not necessarily reflect the views of the National Science Foundation.

Institutional Review Board Statement: Not applicable.

Informed Consent Statement: Not applicable.

Data Availability Statement: The original contributions presented in this study are included in the article/Supplementary Material. Further inquiries can be directed to the corresponding author.

Conflicts of Interest: The authors firmly affirm that there are no conflicts of interest.

References

1. Roy, J. (Ed.) 4—Bulk drugs or active pharmaceutical ingredients. In *An Introduction to Pharmaceutical Sciences*; Woodhead Publishing: Sawston, UK, 2011; pp. 69–109.
2. Mantri, R.; Sanghvi, R. Solubility of pharmaceutical solids. In *Developing Solid Oral Dosage Forms*; Elsevier: Amsterdam, The Netherlands, 2017; pp. 3–22.
3. Ghadi, R.; Dand, N. BCS class IV drugs: Highly notorious candidates for formulation development. *J. Control. Release* **2017**, *248*, 71–95. [CrossRef] [PubMed]
4. Naing, M.D.; Tsume, Y. Dissolution profiles of BCS class II drugs generated by the gastrointestinal simulator alpha has an edge over the compendial USP II method. *Eur. J. Pharm. Biopharm.* **2024**, *203*, 114436. [CrossRef] [PubMed]
5. Bhalani, D.V.; Nutan, B.; Kumar, A.; Singh Chandel, A.K. Bioavailability Enhancement Techniques for Poorly Aqueous Soluble Drugs and Therapeutics. *Biomedicines* **2022**, *10*, 2055. [CrossRef]
6. Papadopoulou, V.; Valsami, G.; Dokoumetzidis, A.; Macheras, P. Biopharmaceutics classification systems for new molecular entities (BCS-NMEs) and marketed drugs (BCS-MD): Theoretical basis and practical examples. *Int. J. Pharm.* **2008**, *361*, 70–77. [CrossRef] [PubMed]
7. Liu, X.; Zhao, L.; Wu, B.; Chen, F. Improving solubility of poorly water-soluble drugs by protein-based strategy: A review. *Int. J. Pharm.* **2023**, *634*, 122704. [CrossRef] [PubMed]
8. Stegemann, S.; Moreton, C.; Svanbäck, S.; Box, K.; Motte, G.; Paudel, A. Trends in oral small-molecule drug discovery and product development based on product launches before and after the Rule of Five. *Drug Discov. Today* **2023**, *28*, 103344. [CrossRef] [PubMed]
9. Sun, D.; Gao, W.; Hu, H.; Zhou, S. Why 90% of clinical drug development fails and how to improve it? *Acta Pharm. Sin. B* **2022**, *12*, 3049–3062. [CrossRef]
10. Kalepu, S.; Nekkanti, V. Insoluble drug delivery strategies: Review of recent advances and business prospects. *Acta Pharm. Sin. B* **2015**, *5*, 442–453. [CrossRef] [PubMed]
11. Savjani, K.T.; Gajjar, A.K.; Savjani, J.K. Drug solubility: Importance and enhancement techniques. *ISRN Pharm.* **2012**, *2012*, 195727. [CrossRef]
12. Williams, H.D.; Trevaskis, N.L.; Charman, S.A.; Shanker, R.M.; Charman, W.N.; Pouton, C.W.; Porter, C.J. Strategies to address low drug solubility in discovery and development. *Pharmacol. Rev.* **2013**, *65*, 315–499. [CrossRef]
13. Jain, J.P.; Leong, F.J.; Chen, L.; Kalluri, S.; Koradia, V.; Stein, D.S.; Wolf, M.C.; Sunkara, G.; Kota, J. Bioavailability of Lumefantrine Is Significantly Enhanced with a Novel Formulation Approach, an Outcome from a Randomized, Open-Label Pharmacokinetic Study in Healthy Volunteers. *Antimicrob. Agents Chemother.* **2017**, *61*, e00868-17. [CrossRef] [PubMed]
14. Dahan, A.; Miller, J.M. The solubility-permeability interplay and its implications in formulation design and development for poorly soluble drugs. *AAPS J.* **2012**, *14*, 244–251. [CrossRef]
15. Zhuo, Y.; Zhao, Y.G.; Zhang, Y. Enhancing Drug Solubility, Bioavailability, and Targeted Therapeutic Applications through Magnetic Nanoparticles. *Molecules* **2024**, *29*, 4854. [CrossRef]
16. Xie, B.; Liu, Y.; Li, X.; Yang, P.; He, W. Solubilization techniques used for poorly water-soluble drugs. *Acta Pharm. Sin. B* **2024**, *14*, 4683–4716. [CrossRef]
17. Khadka, P.; Ro, J.; Kim, H.; Kim, I.; Kim, J.T.; Kim, H.; Cho, J.M.; Yun, G.; Lee, J. Pharmaceutical particle technologies: An approach to improve drug solubility, dissolution and bioavailability. *Asian J. Pharm. Sci.* **2014**, *9*, 304–316. [CrossRef]
18. Subramaniam, B.; Saim, S.; Rajewski, R.A.; Stella, V. Methods for Particle Micronization and Nanonization by Recrystallization from Organic Solutions Sprayed into a Compressed Antisolvent. U.S. Patent 5874029A, 23 February 1999.
19. Shabatina, T.I.; Gromova, Y.A.; Vernaya, O.I.; Soloviev, A.V.; Shabatin, A.V.; Morosov, Y.N.; Astashova, I.V.; Melnikov, M.Y. Pharmaceutical Nanoparticles Formation and Their Physico-Chemical and Biomedical Properties. *Pharmaceuticals* **2024**, *17*, 587. [CrossRef]
20. Esfandiari, N. Production of micro and nano particles of pharmaceutical by supercritical carbon dioxide. *J. Supercrit. Fluids* **2015**, *100*, 129–141. [CrossRef]
21. Vo, C.L.; Park, C.; Lee, B.J. Current trends and future perspectives of solid dispersions containing poorly water-soluble drugs. *Eur. J. Pharm. Biopharm.* **2013**, *85 Pt B*, 799–813. [CrossRef]

22. Nayak, A.K.; Panigrahi, P.P. Solubility enhancement of etoricoxib by cosolvency approach. *Int. Sch. Res. Not.* **2012**, *2012*, 820653. [CrossRef]
23. Loftsson, T. Drug solubilization by complexation. *Int. J. Pharm.* **2017**, *531*, 276–280. [CrossRef]
24. Serajuddin, A.T. Salt formation to improve drug solubility. *Adv. Drug Deliv. Rev.* **2007**, *59*, 603–616. [CrossRef]
25. Almotairy, A.; Almutairi, M.; Althobaiti, A.; Alyahya, M.; Sarabu, S.; Alzahrani, A.; Zhang, F.; Bandari, S.; Repka, M.A. Effect of pH Modifiers on the Solubility, Dissolution Rate, and Stability of Telmisartan Solid Dispersions Produced by Hot-melt Extrusion Technology. *J. Drug Deliv. Sci. Technol.* **2021**, *65*, 102674. [CrossRef] [PubMed]
26. Jin, G.; Ngo, H.V.; Cui, J.H.; Wang, J.; Park, C.; Lee, B.J. Role of Surfactant Micellization for Enhanced Dissolution of Poorly Water-Soluble Cilostazol Using Poloxamer 407-Based Solid Dispersion via the Anti-Solvent Method. *Pharmaceutics* **2021**, *13*, 662. [CrossRef]
27. Sharma, U.; Saroha, K. A Review of Hydrotropic Solubilization Techniques for Enhancing the Bioavailability of Poorly Soluble Drugs. *Int. J. Toxicol.* **2024**, *43*, 63–71. [CrossRef] [PubMed]
28. Cerpnjak, K.; Zvonar, A.; Gašperlin, M.; Vrečer, F. Lipid-based systems as a promising approach for enhancing the bioavailability of poorly water-soluble drugs. *Acta Pharm.* **2013**, *63*, 427–445. [CrossRef]
29. Preeti; Sambhakar, S.; Malik, R.; Bhatia, S.; Al Harrasi, A.; Rani, C.; Saharan, R.; Kumar, S.; Geeta; Sehrawat, R. Nanoemulsion: An Emerging Novel Technology for Improving the Bioavailability of Drugs. *Scientifica* **2023**, *2023*, 6640103. [CrossRef] [PubMed]
30. Shinde, S.S.; Mandake, G.R.; Nitalikar, M.M. Spray Drying: A Promising Technique to Enhance Solubility. *Asian J. Pharm. Technol.* **2018**, *8*, 255–260. [CrossRef]
31. Ainurofiq, A.; Putro, D.S.; Ramadhani, D.A.; Putra, G.M.; Santo, L.D.C.D.E. A review on solubility enhancement methods for poorly water-soluble drugs. *J. Rep. Pharm. Sci.* **2021**, *10*, 137–147. [CrossRef]
32. Mah, P.T.; Peltonen, L.; Novakovic, D.; Rades, T.; Strachan, C.J.; Laaksonen, T. The effect of surfactants on the dissolution behavior of amorphous formulations. *Eur. J. Pharm. Biopharm.* **2016**, *103*, 13–22. [CrossRef]
33. Kumar, V.; Minocha, N.; Garg, V.; Dureja, H. Nanostructured materials used in drug delivery. *Mater. Today Proc.* **2022**, *69*, 174–180. [CrossRef]
34. Mahor, A.; Singh, P.P.; Bharadwaj, P.; Sharma, N.; Yadav, S.; Rosenholm, J.M.; Bansal, K.K. Carbon-based nanomaterials for delivery of biologicals and therapeutics: A cutting-edge technology. *C* **2021**, *7*, 19. [CrossRef]
35. Lohcharoenkal, W.; Wang, L.; Chen, Y.C.; Rojanasakul, Y. Protein nanoparticles as drug delivery carriers for cancer therapy. *BioMed Res. Int.* **2014**, *2014*, 180549. [CrossRef]
36. Aljabali, A.A.; Hassan, S.S.; Pabari, R.M.; Shahcheraghi, S.H.; Mishra, V.; Charbe, N.B.; Chellappan, D.K.; Dureja, H.; Gupta, G.; Almutary, A.G.; et al. The viral capsid as novel nanomaterials for drug delivery. *Future Sci. OA* **2021**, *7*, Fso744. [CrossRef]
37. C Thomas, S.; Kumar Mishra, P.; Talegaonkar, S. Ceramic nanoparticles: Fabrication methods and applications in drug delivery. *Curr. Pharm. Des.* **2015**, *21*, 6165–6188. [CrossRef]
38. Arcos, D.; Vallet-Regi, M. Bioceramics for drug delivery. *Acta Mater.* **2013**, *61*, 890–911. [CrossRef]
39. He, S.; Wu, L.; Li, X.; Sun, H.; Xiong, T.; Liu, J.; Huang, C.; Xu, H.; Sun, H.; Chen, W.; et al. Metal-organic frameworks for advanced drug delivery. *Acta Pharm. Sin. B* **2021**, *11*, 2362–2395. [CrossRef] [PubMed]
40. Karki, S.; Kim, H.; Na, S.-J.; Shin, D.; Jo, K.; Lee, J. Thin films as an emerging platform for drug delivery. *Asian J. Pharm. Sci.* **2016**, *11*, 559–574. [CrossRef]
41. Sun, D.D.; Lee, P.I. Crosslinked hydrogels—A promising class of insoluble solid molecular dispersion carriers for enhancing the delivery of poorly soluble drugs. *Acta Pharm. Sin. B* **2014**, *4*, 26–36. [CrossRef] [PubMed]
42. Jampilek, J.; Kralova, K. Advances in Drug Delivery Nanosystems Using Graphene-Based Materials and Carbon Nanotubes. *Materials* **2021**, *14*, 1059. [CrossRef]
43. Chen, Y.; Chen, H.; Shi, J. Inorganic nanoparticle-based drug codelivery nanosystems to overcome the multidrug resistance of cancer cells. *Mol. Pharm.* **2014**, *11*, 2495–2510. [CrossRef]
44. Chauhan, V.M.; Zhang, H.; Dalby, P.A.; Aylott, J.W. Advancements in the co-formulation of biologic therapeutics. *J. Control. Release* **2020**, *327*, 397–405. [CrossRef] [PubMed]
45. Ataide, J.A.; Coco, J.C.; Dos Santos, É.M.; Beraldo-Araujo, V.; Silva, J.R.A.; de Castro, K.C.; Lopes, A.M.; Filipczak, N.; Yalamarty, S.S.K.; Torchilin, V.P.; et al. Co-Encapsulation of Drugs for Topical Application—A Review. *Molecules* **2023**, *28*, 1449. [CrossRef] [PubMed]
46. Shi, Q.; Moinuddin, S.M.; Cai, T. Advances in coamorphous drug delivery systems. *Acta Pharm. Sin. B* **2019**, *9*, 19–35. [CrossRef]
47. Meng, J.; Guo, F.; Xu, H.; Liang, W.; Wang, C.; Yang, X.D. Combination Therapy using Co-encapsulated Resveratrol and Paclitaxel in Liposomes for Drug Resistance Reversal in Breast Cancer Cells in vivo. *Sci. Rep.* **2016**, *6*, 22390. [CrossRef] [PubMed]
48. Meng, L.; Xia, X.; Yang, Y.; Ye, J.; Dong, W.; Ma, P.; Jin, Y.; Liu, Y. Co-encapsulation of paclitaxel and baicalein in nanoemulsions to overcome multidrug resistance via oxidative stress augmentation and P-glycoprotein inhibition. *Int. J. Pharm.* **2016**, *513*, 8–16. [CrossRef] [PubMed]

49. Tan, A.R.; Im, S.A.; Mattar, A.; Colomer, R.; Stroyakovskii, D.; Nowecki, Z.; De Laurentiis, M.; Pierga, J.Y.; Jung, K.H.; Schem, C.; et al. Fixed-dose combination of pertuzumab and trastuzumab for subcutaneous injection plus chemotherapy in HER2-positive early breast cancer (FeDeriCa): A randomised, open-label, multicentre, non-inferiority, phase 3 study. *Lancet Oncol.* **2021**, *22*, 85–97. [CrossRef] [PubMed]
50. Wang, B.C.; Li, P.C.; Fan, J.Q.; Lin, G.H.; Liu, Q. Durvalumab and tremelimumab combination therapy versus durvalumab or tremelimumab monotherapy for patients with solid tumors: A systematic review and meta-analysis. *Medicine* **2020**, *99*, e21273. [CrossRef]
51. Fule, R.; Dhamecha, D.; Maniruzzaman, M.; Khale, A.; Amin, P. Development of hot melt co-formulated antimalarial solid dispersion system in fixed dose form (ARLUMELT): Evaluating amorphous state and in vivo performance. *Int. J. Pharm.* **2015**, *496*, 137–156. [CrossRef] [PubMed]
52. Chen, H.; Guo, Y.; Wang, C.; Dun, J.; Sun, C.C. Spherical cocrystallization—An enabling technology for the development of high dose direct compression tablets of poorly soluble drugs. *Cryst. Growth Des.* **2019**, *19*, 2503–2510. [CrossRef]
53. Ozenberger, K.; Alexander, G.C.; Shin, J.I.; Whitsel, E.A.; Qato, D.M. Use of prescription medications with cardiovascular adverse effects among older adults in the United States. *Pharmacoepidemiol. Drug Saf.* **2022**, *31*, 1027–1038. [CrossRef]
54. Mueller, C.; Altenburger, U.; Mohl, S. Challenges for the pharmaceutical technical development of protein coformulations. *J. Pharm. Pharmacol.* **2018**, *70*, 666–674. [CrossRef] [PubMed]
55. Karagianni, A.; Kachrimanis, K.; Nikolakakis, I. Co-Amorphous Solid Dispersions for Solubility and Absorption Improvement of Drugs: Composition, Preparation, Characterization and Formulations for Oral Delivery. *Pharmaceutics* **2018**, *10*, 98. [CrossRef]
56. Malaie, K.; Ganjali, M.R. Spinel nano-ferrites for aqueous supercapacitors; linking abundant resources and low-cost processes for sustainable energy storage. *J. Energy Storage* **2021**, *33*, 102097. [CrossRef]
57. Maghsoodi, M.; Kiafar, F. Co-precipitation with PVP and Agar to Improve Physicomechanical Properties of Ibuprofen. *Iran. J. Basic Med. Sci.* **2013**, *16*, 635–642. [PubMed]
58. Zhang, J.; Liu, M.; Zeng, Z. The antisolvent coprecipitation method for enhanced bioavailability of poorly water-soluble drugs. *Int. J. Pharm.* **2022**, *626*, 122043. [CrossRef]
59. Islam, M.S.; Renner, F.; Azizighannad, S.; Mitra, S. Direct incorporation of nano graphene oxide (nGO) into hydrophobic drug crystals for enhanced aqueous dissolution. *Colloids Surf. B Biointerfaces* **2020**, *189*, 110827. [CrossRef]
60. Chen, K.; Mitra, S. Incorporation of functionalized carbon nanotubes into hydrophobic drug crystals for enhancing aqueous dissolution. *Colloids Surf. B Biointerfaces* **2019**, *173*, 386–391. [CrossRef] [PubMed]
61. Islam, M.S.; Mitra, S. Microwave Synthesis of Nanostructured Functionalized Polylactic Acid (nfPLA) for Incorporation into a Drug Crystals to Enhance Their Dissolution. *J. Pharm. Sci.* **2023**, *112*, 2260–2266. [CrossRef] [PubMed]
62. Islam, M.S.; Mitra, S. Synthesis of Microwave Functionalized, Nanostructured Polylactic Co-Glycolic Acid (nfPLGA) for Incorporation into Hydrophobic Dexamethasone to Enhance Dissolution. *Nanomaterials* **2023**, *13*, 943. [CrossRef]
63. Shahriari, S.; Sastry, M.; Panjikar, S.; Singh Raman, R.K. Graphene and Graphene Oxide as a Support for Biomolecules in the Development of Biosensors. *Nanotechnol. Sci. Appl.* **2021**, *14*, 197–220. [CrossRef]
64. Ghulam, A.N.; Dos Santos, O.A.L.; Hazeem, L.; Pizzorno Backx, B.; Bououdina, M.; Bellucci, S. Graphene Oxide (GO) Materials-Applications and Toxicity on Living Organisms and Environment. *J. Funct. Biomater.* **2022**, *13*, 77. [CrossRef] [PubMed]
65. Amin, M.K.; Boateng, J. Surface functionalization of PLGA nanoparticles for potential oral vaccine delivery targeting intestinal immune cells. *Colloids Surf. B Biointerfaces* **2023**, *222*, 113121. [CrossRef] [PubMed]
66. Li, X.; Wei, Y.; Wen, K.; Han, Q.; Ogino, K.; Ma, G. Novel insights on the encapsulation mechanism of PLGA terminal groups on ropivacaine. *Eur. J. Pharm. Biopharm.* **2021**, *160*, 143–151. [CrossRef] [PubMed]
67. Félix Lanao, R.P.; Jonker, A.M.; Wolke, J.G.; Jansen, J.A.; van Hest, J.C.; Leeuwenburgh, S.C. Physicochemical properties and applications of poly(lactic-*co*-glycolic acid) for use in bone regeneration. *Tissue Eng. Part B Rev.* **2013**, *19*, 380–390. [CrossRef]
68. Ding, Y.; Cui, W.; Zhang, Z.; Ma, Y.; Ding, C.; Lin, Y.; Xu, Z. Solubility and Pharmacokinetic Profile Improvement of Griseofulvin through Supercritical Carbon Dioxide-Assisted Complexation with HP-γ-Cyclodextrin. *Molecules* **2023**, *28*, 7360. [CrossRef] [PubMed]
69. Stefánsson, E.; Loftsson, T. CHAPTER 13—Microspheres and nanotechnology for drug delivery. In *Retinal Pharmacotherapy*; Nguyen, Q.D., Rodrigues, E.B., Farah, M.E., Mieler, W.F., Eds.; W.B. Saunders: Philadelphia, PA, USA, 2010; pp. 86–90.
70. Food and Drug Administration. *Memorandum and Product Quality Review: NDA 211379 for Hemady (Dexamethasone) Immediate Release Tablets, 20 mg*; Center for Drug Evaluation and Research, Department of Health and Human Services: Beltsville, MD, USA, 2019.
71. Glomme, A.; März, J.; Dressman, J.B. Comparison of a Miniaturized Shake-Flask Solubility Method with Automated Potentiometric Acid/Base Titrations and Calculated Solubilities. *J. Pharm. Sci.* **2005**, *94*, 1–16. [CrossRef] [PubMed]
72. Baka, E.; Comer, J.E.A.; Takács-Novák, K. Study of equilibrium solubility measurement by saturation shake-flask method using hydrochlorothiazide as model compound. *J. Pharm. Biomed. Anal.* **2008**, *46*, 335–341. [CrossRef] [PubMed]

73. Islam, M.S.; Renner, F.; Foster, K.; Oderinde, M.S.; Stefanski, K.; Mitra, S. Hydrophilic and Functionalized Nanographene Oxide Incorporated Faster Dissolving Megestrol Acetate. *Molecules* **2021**, *26*, 1972. [CrossRef]
74. Islam, M.S.; Mitra, S. Effect of nano graphene oxide (nGO) incorporation on the lipophilicity of hydrophobic drugs. *Hybrid Adv.* **2023**, *3*, 100074. [CrossRef]
75. Brown, W.E.; Marques, M.R. USP and dissolution—20 Years of progress. *Dissolut Technol.* **2014**, *2014*, 24–27. [CrossRef]
76. Gray, V.A. Dissolution Testing in the Pharmaceutical Laboratory. In *Analytical Testing for the Pharmaceutical GMP Laboratory*; Wiley Online Library: Hoboken, NJ, USA, 2022; pp. 206–250.
77. Gray, V.A.; Rosanske, T.W. Dissolution. In *Specification of Drug Substances and Products*; Elsevier: Amsterdam, The Netherlands, 2020; pp. 481–503.
78. Scimeca, M.; Bischetti, S.; Lamsira, H.K.; Bonfiglio, R.; Bonanno, E. Energy Dispersive X-ray (EDX) microanalysis: A powerful tool in biomedical research and diagnosis. *Eur. J. Histochem.* **2018**, *62*, 2841. [CrossRef] [PubMed]
79. Azaroon, M.; Kiasat, A.R. Silver nanoparticles engineered β-cyclodextrin/γ-Fe_2O_3@ hydroxyapatite composite: Efficient, green and magnetically retrievable nanocatalyst for the aqueous reduction of nitroarenes. *Catal. Lett.* **2018**, *148*, 745–756. [CrossRef]
80. Rask, M.B.; Knopp, M.M.; Olesen, N.E.; Holm, R.; Rades, T. Comparison of two DSC-based methods to predict drug-polymer solubility. *Int. J. Pharm.* **2018**, *540*, 98–105. [CrossRef]
81. Saganowska, P.; Wesolowski, M. DSC as a screening tool for rapid co-crystal detection in binary mixtures of benzodiazepines with co-formers. *J. Therm. Anal. Calorim.* **2018**, *133*, 785–795. [CrossRef]